

Duquesne University

Duquesne Scholarship Collection

Electronic Theses and Dissertations

Spring 5-7-2021

Detecting a Heterogenous Sample of Pigmented Melanoma Cell Lines Using Photoacoustic Flow Cytometry

Margaret Cappellano

Follow this and additional works at: <https://dsc.duq.edu/etd>



Part of the [Bioimaging and Biomedical Optics Commons](#)

Recommended Citation

Cappellano, M. (2021). Detecting a Heterogenous Sample of Pigmented Melanoma Cell Lines Using Photoacoustic Flow Cytometry (Master's thesis, Duquesne University). Retrieved from <https://dsc.duq.edu/etd/1967>

This Immediate Access is brought to you for free and open access by Duquesne Scholarship Collection. It has been accepted for inclusion in Electronic Theses and Dissertations by an authorized administrator of Duquesne Scholarship Collection.

DETECTING A HETEROGENOUS SAMPLE OF PIGMENTED MELANOMA CELL
LINES USING PHOTOACOUSTIC FLOW CYTOMETRY

A Thesis

Submitted to the Rangos School of Health Sciences

Duquesne University

In partial fulfillment of the requirements for
the degree of Master of Science

By

Margaret Cappellano

May 2021

Copyright by
Margaret Cappellano

2021

DETECTING A HETEROGENOUS SAMPLE OF PIGMENTED MELANOMA CELL LINES
USING PHOTOACOUSTIC FLOW CYTOMETRY

By

Margaret Cappellano

Approved March 25, 2021

Dr. John Viator
Chair, Department of Engineering
(Committee Chair)

Dr. Bin Yang
Professor of Engineering
(Committee Member/ Reader)

Dr. Gerard Magill
Professor of Healthcare Ethics
(Committee Member/ Reader)

Dr. Fevzi Akinci
Dean, Rangos School of Health Sciences
Professor of Chemistry and Biochemistry

ABSTRACT

DETECTING A HETEROGENOUS SAMPLE OF PIGMENTED MELANOMA CELL LINES USING PHOTOACOUSTIC FLOW CYTOMETRY

By

Margaret Cappellano

May 2021

Thesis supervised by Dr. John Viator

Metastatic melanoma is the deadliest form of skin cancer, which is in part, attributed to its rapid aggression and lack of response to typical treatment methods. There are far too often cases where a lymph node biopsy does not detect the severity of the cancer, which in turn causes a lack of diagnosis until a mass can be visually detected on a scan, such as a PET, CT, or MRI. Once visible on a scan, the cancer is too progressive for successful treatment. To avoid this, we investigated how a blood sample can be used to negate a missed diagnosis, by using photoacoustic flow cytometry to detect melanoma cells within the blood. We studied the absorbance wavelength of human melanoma cells to determine the ideal cellular characteristics needed for photoacoustic flow cytometry detection. Using this data, we also determined the viability of a heterogenous melanoma cell sample being accurately detected through the flow chamber. These novel findings will be further used to develop photoacoustic flow cytometry as a

viable, accurate, and timely method of melanoma detection and monitoring. They will also be used to further understand a minimum cell concentration and absorption reading needed for photoacoustic detection.

ACKNOWLEDGMENT

I would like to thank Dr. John Viator for continued support, direction, and guidance throughout my undergraduate, graduate and research career. Not only did Dr. Viator provide knowledge, and critical feedback, he continually challenged my own ideas and abilities, catalyzing higher arguments and skill sets. Dr. Viator's unwavering support, and resources truly are a testament to his character and his students' success.

In addition to Dr. Viator, special thanks to Dr. Gerard Magill and Dr. Bin Yang for being on the defense board for this thesis. I have greatly enjoyed their instruction inside and outside of the classroom and was honored to have them as a part of this process.

I would also like to thank Isabella McCollum, a first- year undergraduate student here at Duquesne University. Isabella is an eager student both inside and outside of the lab. Her attention to detail, hard work, and curiosity lead to a great partnership. She was able to oversee the research process, lend a hand with sample preparation, culture care, and provide new and refreshing ideas along the way. I am excited to see where her bright future takes her inside of the lab.

Dr. Kimberly Williams played a pivotal role in the planning, and execution of my thesis. Thank you, Dr. Williams, for your continued guidance and support through keeping me organized, on schedule, and motivated.

To those who have performed other exemplary research into similar topics, I thank you for your work. You provided me with challenging perspectives, and information that played vital roles in my methods and procedures.

Lastly, I would like to thank my friends and family. Their support, and motivation has been vital in this process. Thank you for believing in me, my abilities, and my future. To my Mom, Dad, and sister Madison, thank you for keeping my spirits high and positive despite the many stressful, long nights. Thank you for showing me what hard work and determination look like, and always reminding me that I can do anything I put my mind to.

TABLE OF CONTENTS

	Page
Abstract.....	iii
Acknowledgement.....	v
List of Figures.....	ix
Chapter 1: Introduction to Melanoma.....	1
1.1: Optical Absorption.....	6
1.2: Photoacoustics.....	9
1.3: Current and Historical Investigations.....	12
1.4: Purpose.....	14
Chapter 2: Methods.....	17
2.1: Media.....	17
2.2: Cell Culture.....	17
2.3: Absorption.....	18
2.3: Increasing Melanin Concentration.....	20
2.4: Heterogenous Culture.....	21
2.5: Photoacoustic Flow Cytometry.....	21
Chapter 3: Results.....	24
3.1: Optimization of Cellular Absorption for Flow Cytometry Detection.....	24
3.2: Determining Heterogenous CTC Detection.....	26
Chapter 4: Discussion.....	26
4.1: Future Advancements.....	27
4.2: Conclusions.....	29

Appendix.....	31
---------------	----

LIST OF FIGURES

	Page
Figure 1: The Clark Model, which illustrates the progression of melanocytes to melanoma. The melanocytes form nevi, which develops into dysplasia, hyperplasia, invasion, and eventually metastasis [2]	1
Figure 2: Biologic events and molecular changes in the progression of melanoma. Not only is the basement membrane penetrated by the melanoma cells, but the melanoma also grows intradermally as an expanding nodule [14]	3
Table 1: All genes were used to compute the Pearson's correlation of all the cell line- malignant cell pairs. The cell lines were ranked based on their average correlation indicated malignant cells (n=1256). MITF and AXL program enriched cells represent the cells with the highest and lowest 400 MITF/ AXL enriched cell, respectively. MITF or AXL gene set enrichment is indicated based on GAGE analyses. MITF, AXL or intermediate clusters were structured based on Gaussian Kernels [65]	4
Figure 3: Diagram of simple beam spectrometer [70].....	6
Figure 4: (a) Absorption spectrum of the same solution in different concentrations of water. Illustrates direct correlation between absorbance and concentration. (b) Calibrations curve of the sample is water [69].....	7
Figure 5: How to evaluate a photoacoustic signal [61]	10
Figure 6: (a) Rabbit used in the experiment conducted by Amar et al. (b) Opto- acoustic traces from the rabbit's retina using a pulsed laser detector [48]	13
Figure 7: Newly cultured HTB-71 cells, generation zero.....	17

Figure 8: Microplate reader diagram. The microplate is loaded into the machine, where a Flashlamp illuminates light onto the well- plate, and the spectrometer detector deduces how much of the original light is transmitted. The absorbance is computed and converted to a visual representation on the computer [70]	19
Figure 9: Microscopic image of not stuck, and stuck HS936 cells.....	20
Figure 10: Schematic of the photoacoustic flow chamber.....	22
Figure 11: Top- view of the photoacoustic flow chamber, where the two orange wires on the left are the alternating flow tubes creating two phase flow generation through the quartz tube. The blue fiber optic wire introduces the flow chamber to the flashing light, catalyzing acoustic waves from cell interaction.....	23
Figure 12: Two phase flow generation system.....	23
Table 2: Melanin concentration of various melanoma cell lines, before and after catalyzing melanogenesis.....	24
Graph 1: Melanin concentration of various melanoma cell lines, before and after catalyzing melanogenesis.....	24
Table 3: Number of melanoma cells detected, using photoacoustic flow cytometry, of untreated and UV treated cell lines.....	25
Graph 2: Number of melanoma cells detected, using photoacoustic flow cytometry, of untreated and UV treated cell lines.....	25

CHAPTER 1: INTRODUCTION TO MELANOMA

Simply defined, melanoma is cancer of the melanocyte, the melanin producing cells of the epidermis and hair follicles. Melanoma is a relatively intractable cancer, proven by the lack of understanding associated with the mechanisms that hinder the effectiveness of chemotherapy. In relation to all dermatologic cancers, melanoma accounts for four percent of all diagnoses, yet is responsible for eighty percent of yearly deaths; where only fourteen percent of patients diagnosed with metastatic melanoma live longer than five years [1].

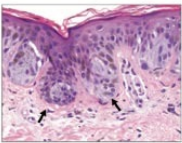
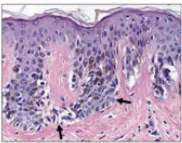
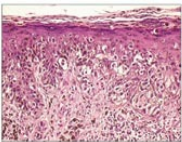
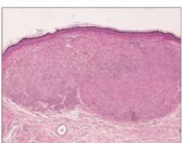
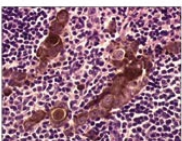
Histopathological Appearance	Description	Histologic Features
 <p>Benign nevus</p>	<p>Step 1</p> <p>The first event is a proliferation of structurally normal melanocytes leading to the benign nevus. Clinically, these nevi present as flat or slightly raised lesions with either uniform coloration or a regular pattern of dot-like pigment in a tan or dark brown background. Histologically, such lesions have an increased number of nested melanocytes along the basal layer (arrows).</p>	<p>Proliferation of melanocytes</p> <p>Benign lesions</p>
 <p>Dysplastic nevus</p>	<p>Step 2</p> <p>The next step is the development of aberrant growth. This may occur within a preexisting benign nevus or in a new location. Clinically such lesions may be asymmetric, have irregular borders, contain multiple colors, or have increasing diameters. Histologically, such lesions have random and discontinuous cytologic atypia (arrows).</p>	<p>Dysplastic cells</p> <p>Random atypia</p>
 <p>Radial-growth phase</p>	<p>Step 3</p> <p>During the radial-growth phase, cells acquire the ability to proliferate intraepidermally. Clinically, they sometimes present as raised lesions. These lesions no longer display random atypia and instead show cytomorphic cancer throughout the lesion. In addition to the intraepidermal cancer, the cells can penetrate the papillary dermis singly or in small nests but fail to form colonies in soft agar.</p>	<p>Intraepidermal growth</p> <p>Continuous atypia</p>
 <p>Vertical-growth phase</p>	<p>Step 4</p> <p>Lesions that progress to the vertical-growth phase acquire the ability to invade the dermis and form an expansile nodule, widening the papillary dermis. The cells can also extend into the reticular dermis and fat, are capable of growth in soft agar, and have the capacity to form tumor nodules when implanted in nude mice.</p>	<p>Dermal invasion</p>
 <p>Metastatic melanoma</p>	<p>Step 5</p> <p>The final step in the model is the successful spread of cells to other areas of the skin and other organs, where they can successfully proliferate and establish a metastatic focus. These cells can grow in soft agar and can form tumor nodules that may metastasize when implanted in nude mice.</p>	<p>Metastasis</p>

Figure 1: The Clark Model, which illustrates the progression of melanocytes to melanoma. The melanocytes form nevi, which develops into dysplasia, hyperplasia, invasion, and eventually metastasis [14]. Reproduced with permission from (scientific reference citation), Copyright Massachusetts Medical Society.

The Clark Model illustrates the histological changes which occur to transform melanocytes to malignant melanoma. The first phenotypic change is seen when the melanocytes develop nevi, which are an alternative type of melanocyte [2]. Growth of the nevi begins when an abnormal activation of the mitogen, a small protein that catalyzes cell division, occurs in the melanoma cell [3]. The activation of the mitogen is a result of a somatic mutation of N-RAS (protein involved with regulating cell division), called BRAF [4]. In a study performed on zebrafish, the expression of a mutant BRAF, in conjunction with the lack of activation in the tumor-suppressor gene, caused malignant melanoma [5]. Next, the development of cytologic atypia occurs within the nevi present in the melanocyte. In this stage, DNA repair, cell growth, and susceptibility to cell death, occurs [6]. This is due to the activation failure of the tumor-suppressor gene, like CDKN2A or PTEN. Thus, the nevi will become malignant or increase the rate of development of melanoma [7]. In a healthy melanocyte, differentiation, and the expression of genes which encode proteins for pigment production are aided by the microphthalmia-associated transcription factor (MITF) [8]. A relatively unknown anomaly in the development of melanoma, is the role of MITF. Usually, MITF is responsible for the expression of SILV and MLANA, which are melanocyte-lineage genes, but are absent in melanoma. However, MITF is still expressed and present in nearly all melanomas [9]. Thus, it can be deduced that the expression of MITF in conjunction with BRAF, as earlier discussed, could affect primary melanocyte cultures, making MITF an oncogene [10].

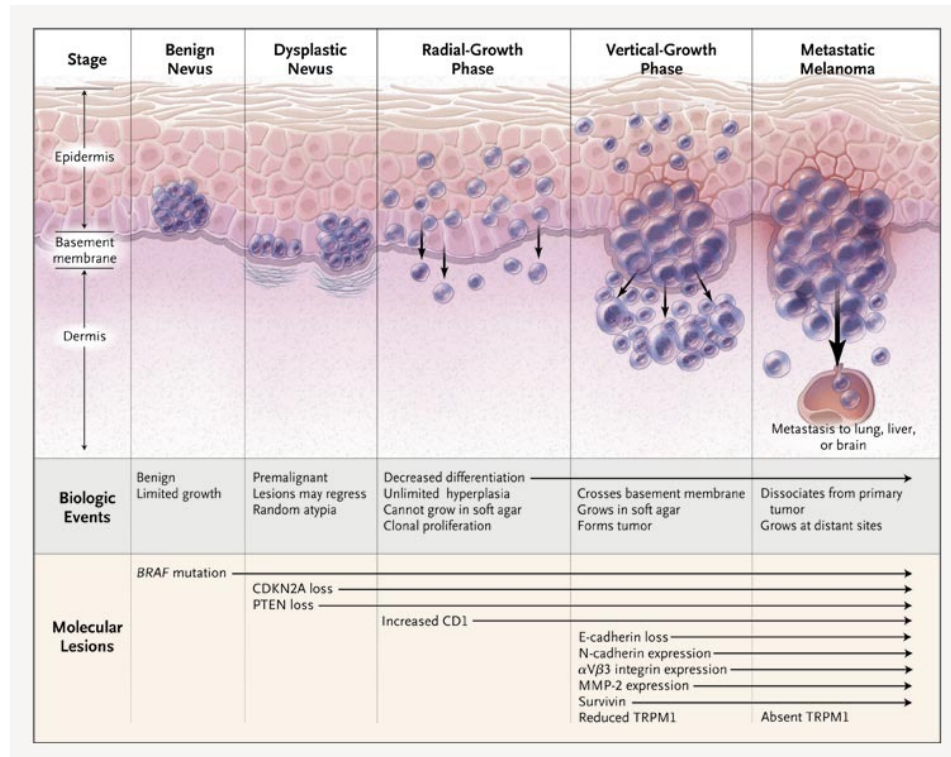


Figure 2: Biologic events and molecular changes in the progression of melanoma. Not only is the basement membrane penetrated by the melanoma cells, but the melanoma also grows intradermally as an expanding nodule [14]. Reproduced with permission from (scientific reference citation), Copyright Massachusetts Medical Society.

Metastatic cancers' invasion and spread are heavily responsible for the high mortality rates, including melanoma. The Clark Model states that metastatic melanoma's invasive characteristics include vertical- growth through the basement membrane. Metastatic melanoma begins when a tumor cell travels from the primary location and migrates. It can travel through the stroma, and thus contaminate blood vessels and the lymphatic system to begin new tumors [11]. The depth of the primary invasion, in conjunction with a histological analysis, provides the evidence for diagnostic and staging purposes. A lack of cell adhesion is what causes the tumor cells to migrate from the primary lesion. Disturbances in this cell adhesion process thus contributes to the metastasizing process. Cadherins are the proteins within the cell membrane which catalyze cell adhesion, through actin cytoskeleton connections and intracellular signaling.

Errors in cadherin expression thus induce melanoma survival and proliferation [12]. The increase radial- growth rate which leads to more vertical- growth of the melanoma, is attributed to a decrease in epithelial cadherin, and an increase in neural cadherin. Unfortunately, neural cadherin is a common characteristic of invasive melanoma, and enables metastatic spread through dermal fibroblasts and the vascular endothelium [13].

Three melanoma cell lines were chosen for investigation. It is important to understand why these specific cell lines were chosen, and what their differences are. Primarily, their differences are attributed to transcriptomes, tumor purity, UV mutational signatures and the expression of skin- associated genes [64]. The ranking system used illustrates the most similar to patient tumors, to least similar, respectively.

	Mean correlation to					
	All malignant tumor cells	The top MITF program enriched malignant cells	The top AXL program enriched malignant cells	Cell line MITF gene set enrichment	Cell line AXL gene set enrichment	Predominant MITF/ AXL cluster
COLO 849	0.542	0.530	0.508	2.96	-0.39	MITF
HTB- 71	0.514	0.437	0.514	0.46	3.20	Intermediate
HS936	0.505	0.554	0.456	2.34	-2.22	MITF
SK- MEL- 3	0.465	0.532	0.410	2.37	-0.44	MITF

HS839	0.216	0.189	0.224	-2.70	2.36	AXL
-------	-------	-------	-------	-------	------	-----

Table 1: All genes were used to compute the Pearson's correlation of all the cell line- malignant cell pairs. The cell lines were ranked based on their average correlation indicated malignant cells (n=1256). MITF and AXL program enriched cells represent the cells with the highest and lowest 400 MITF/ AXL enriched cell, respectively. MITF or AXL gene set enrichment is indicated based on GAGE analyses. MITF, AXL or intermediate clusters were structured based on Gaussian Kernels. [64]

In a study conducted by Tirosh et al., the RNA- sequencing of 4,000 malignant melanoma cells from tumors was found [65]. This data was useful to find which cell lines are most transcriptionally similar to their malignant cells versus all the cells from the tumor. Thus, it is possible to directly compare the transcriptomes of the cell's lines and malignant melanoma cells directly from tumors. The top ranked cell line, COLO 849 has the highest correlation coefficient, as compared to HS839 with the lowest correlation coefficient [64].

It has also been found that there are two main transcriptional signatures that define melanoma. First, the proliferative stage, which is determined by MITF expression, and the invasive state. Further findings illustrates that the first stage can be further defined by MITF and AXL gene programs. Thus, the selected melanoma cell lines differ in their expression of the gene sets. An enrichment analysis of MITF and AXL gene sets was conducted and a cluster analysis deduced the enrichment values, defined by high MITF expression, high AXL expression and an intermediate group. An analysis of the average correlation coefficient of MITF or AXL gene sets illustrated either high or low representations of one transcriptional state, but not both. For example, Table 1 illustrates how SK-MEL-3 correlates well with MITF enriched cells [$r= 0.532$] but poorly with AXL enriched cells [$r= 0.410$] [64].

1.1 OPTICAL ABSORPTION

When electromagnetic energy is transformed into internal energy, like thermal energy, it can be described as the absorption of electromagnetic radiation by matter. In optical absorption, the medium's transparency changes with the light wave intensity, which causes saturable absorption, or nonlinear absorption [56].

Spectroscopy is a method concerned with the absorption, emission and scattering of electromagnetic radiation by atoms or molecules [57]. This method can deduce the absorbance of each melanoma sample, where the greater the absorbance, the higher melanin content the particular sample has. Once the sample is loaded into the spectrometer, a light is directed through a fiber optic cable through a narrow aperture, called an entrance slit. This slit is able to vignette the light as it enters, where it is then collimated by a concave mirror onto a grating. The grate then disperses the light through various angles, where it is then focused by a second concave mirror onto the detector. From the detector, the light photons are converted into electrons and digitized to a computer. The computer interpolates the signal over a given wavelength and deduces a spectral range of absorbance. The data can be manipulated for countless other applications outside of absorbance [58]. By knowing the absorbance of a sample, a specific light wavelength can be chosen to detect the needed characteristics of the sample.

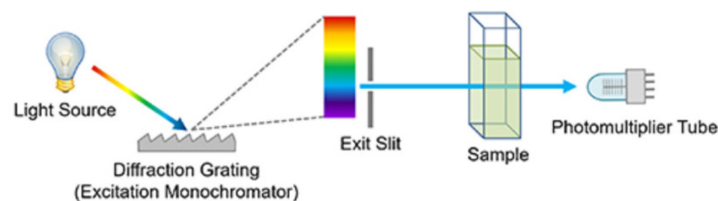


Figure 3: Diagram of simple beam spectrometer [69].

It is important to note that absorbance is a unitless measurement, which can be understood through Beer's Law. This law states that the absorbance is proportional to the path length through the sample and the concentration of the absorbing species [67]. More specifically,

$$A = \epsilon cl$$

Where,

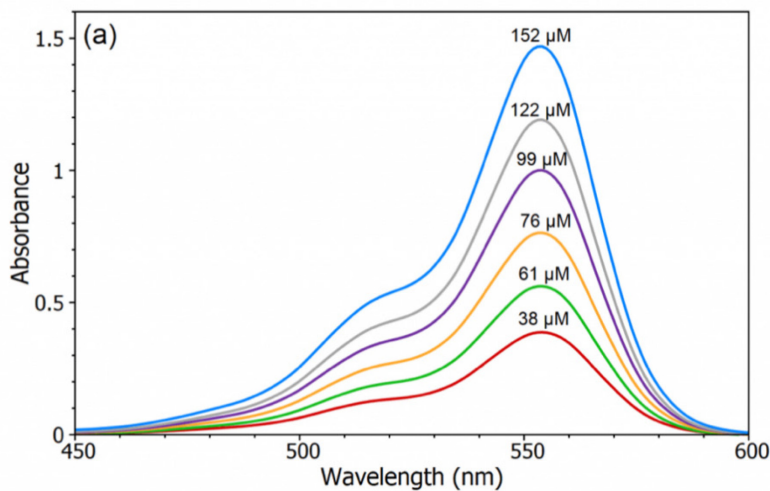
A = absorbance

ϵ = molar absorption coefficient

c = molar concentration

l = optical path length

The units of ϵ are $M^{-1}cm^{-1}$ which is multiplied by the units of molar concentration and optical path length, M and cm, respectively. Thus, absorbance is a unitless dimension. The molar absorption coefficient is a measure of how well a sample absorbs light at a particular wavelength. Ultimately, the law states that there is a linear relationship between the absorbance and concentration of a sample [68].



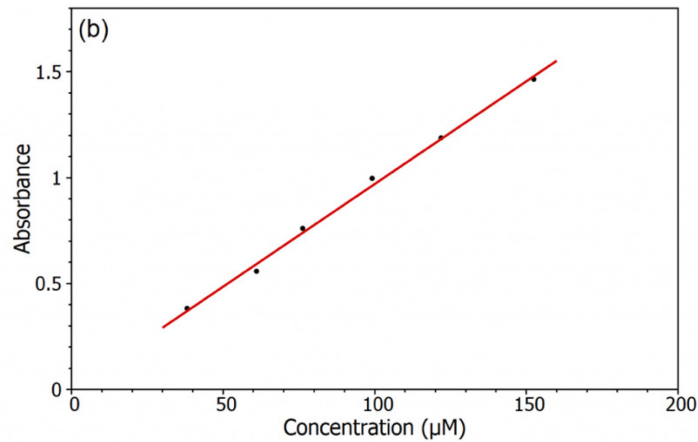


Figure 4: (a) Absorption spectrum of the same solution in different concentrations of water. Illustrates direct correlation between absorbance and concentration. (b) Calibrations curve of the sample in water [68].

Saturable absorbance can be defined by matter absorbing light, which is reduced at high optical intensities. In this specific application of photoacoustics, the laser light is consistently pulsed. Due to the pulsation of the light, there are fast saturable absorbers, and slow absorbers. A fast saturable absorber has a medium with a recovery time below the duration of the laser pulse, where a slow absorber has a medium with a recovery time above the pulse duration [56].

The light seen in a laser beam holds various characteristics that differ it from ordinary light. First, light in a laser beam is directed in a straight line, where ordinary light, like a light bulb, is directed in waves of many directions. The single wavelength of a laser, also referred to as monochromaticity is unique when compared to the varying wavelengths of ordinary light, that when combined, appear white. Coherence can be defined as the interaction between light waves in terms of their peaks and troughs. Laser beam coherence is synchronized, when the peaks and troughs line up, which is unlike ordinary light [60].

Typically, in melanoma research, a wavelength of 532 nm is used for a variety of reasons. After the laser hits the sample, the wavelength that is deflected is absorbed by the retina, displaying a color characteristic. The visible rays or wavelengths are 400 to 700nm, where 532 nm falls generally in the middle of the short and long wavelengths. Any wavelength outside of these boundaries are no longer visible rays and cannot be seen by the human eye. Second, Harmonic Generation (SHG) is half of the typical 1064 nm wavelength, thus 532 nm. A wavelength of 1064 nm is the primary wavelength used in an Nd: YAG (neodymium- doped yttrium aluminum garnet) laser, which is an extremely common type of laser used in photoacoustics. It is produced by using a nonlinear KTP crystal to reduce the original 1064 nm. It has high peak power, without large amounts of heat transfer, and is often used for intricate processing due to its smaller beam spot in comparison to other IR lasers [60]. In addition, 532 nm lasers are readily available off the shelf, and are highly cost effective. They are heavily used in fluorescence spectroscopy, optical alignment, and dermatology.

1.2 PHOTOACOUSTICS

Simply defined, photoacoustics is the creation of acoustic waves due to light absorption. When a pulsed laser light hits matter, in this case a circulating melanoma cell (CMC), thermoelastic expansion of the cell occurs. The cell absorbs part of the laser light energy, which produces an increase in internal cell temperature. When matter absorbs heat, it expands. This expansion produces a pressure wave [15]. Sometimes, the pressure wave is so great, the matter begins to oscillate, or move around a central point. This oscillation produces a sound wave, which is 50-5000 times greater than what a human ear can detect. In order to do so, the laser pulses at a sound frequency of 1-1000MHz [16,17]. Within the laser setup there is a transducer

which detects the acoustic wave. An oscilloscope will then process the data from the transducer and display it through a graphical waveform on a screen [18].

In order to create the pressure oscillation, the matter must be heated and cooled. This can be done through a modulated excitation or pulsed excitation. In modulated excitation, a sine or square wave is formed due to radiation sources of fluctuating intensity [19-23]. On the other hand, pulsed excitation uses nanosecond flashes of the laser. This causes a short sample illumination, proceeded by a longer dark cycle. Thus, the oscilloscope is able to process the thermal expansion. For a singular frequency, a modulated excitation is preferred, but for multiple acoustic waves, which was chosen for this experiment, pulsed excitation is used [24].

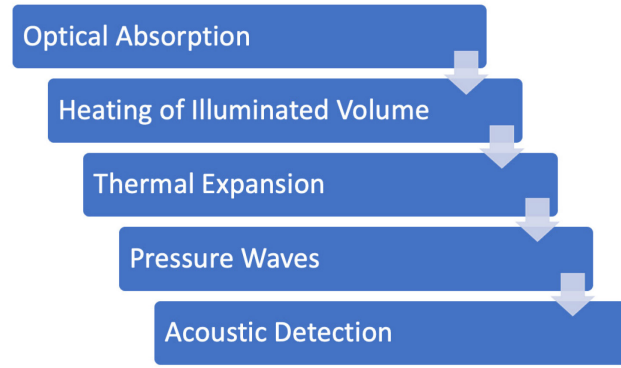


Figure 5: How to evaluate a photoacoustic signal

The acoustic signal generated inside the cell, detected using a microphone, has an amplitude defined by,

$$\rho = FW_0\mu_0$$

Where,

W_0 = Incident radiation power

μ_0 = Absorption coefficient of the sample

F = The proportionality factor, defined by

$$F = G(\gamma - 1)L/\gamma V$$

Where,

G = Geometric factor of the order of one

γ = Adiabatic coefficient of the gas

L = Length of the cell

V = Volume of the cell

The generated photoacoustic signal is indirectly proportional to the modulation frequency and cross section of the cell, thus as the cell decreases in size and modulation frequency, the signal increases [25-28]. The modulation frequency is then defined as,

$$\omega = 2\pi\nu$$

The short laser pulses lead to the expansion of the cell and pressure pulses. These pressure pulses are detected through optical methods or piezoelectric transducers. The depth of the pulses is then dependent on the time resolution of the transducer. This is calculated by multiplying the speed of sound on the sample and the product of the temporal resolution [25-28]. The depth ranges from micrometer to centimeters, which is affected by the rate of absorbance or scattering of the sample. In comparison to other optical techniques, such as absorption spectroscopy, photoacoustics are more desirable due to the pressure waves being detected and generated through a direct source of absorbed energy. In absorption spectroscopy, the absorbances are indirectly detected by reflectance or transmittance [29,30]. Thus, photoacoustic imaging produces a higher resolution outcome, in conjunction with maintaining a high level of contrast, which is why it is an advantageous method in melanoma cell detection.

1.3 CURRENT AND HISTORICAL INVESTIGATIONS

In 1876, Alexander Bell began to study the use of light in the transmission of speech [31]. Through his work, he developed the photophone, which was the first speech transmission by light. The sound within the telephone circuit was voice- modulated light intensities converted through the battery current. This technology is considered the first implementation of wireless telephony, or the first optical communication device. More importantly, Bell discovered that the illumination of different solid substances with a rapidly interrupted beam of light energy results in the emission of acoustic energy at the same frequency as the modulated frequency [31]. With this conclusion, he was able to replace the selenium- cell in the photophone, with a lamp- black receiver. Thus, the light modulations were directly converted into speech [32]. This effect was dubbed the “sonorous” effect and studied heavily by other notable scientists.

Lord Rayleigh concluded that the sound was due to a vibration caused by the unequal heating of the plates when pulsed with light [33]. Mercadier and Preece postulated that the sound waves were due to vibration, rather the expansion and contraction due to the air contact heating the disk [34-36]. Though use of the photophone in a practical sense was difficult, as it relied on human hearing, it was still a phenomenal finding that illustrated using light to replace electrical signals as an information carrier. Decades later, this effect was further developed by Veingerov of the State Optical Institute of Leningrad [37]. Through infrared gas analysis, and understanding the principle of the photophone, Veingerov was able to detect CO₂ concentrations using charged capacitive microphone diaphragms. Pfund further expanded on this, stating that the system directly measured the changes of gas temperature, instead of pressure changes [38]. This phenomenon was dubbed the opto- acoustic effect, as two tubes became joined in a coupled chamber, separated by a membrane capacitor which acted as a microphone. Infrared sources then

interrupted the chamber by a rotating disk, where acoustic signals were generated and measured as a differential signal through a microphone [39-44].

In 1960, the laser was developed which illustrated a revival of new phenomena. Kerr and Atwood measured gas absorbances using pulsed laser lights, in conjunction with acoustic detection using a capacitance microphone [45]. The piezoelectric effect, developed by Pierre and Jacques Curie in 1880, was then applied to the gas- microphone, as it was more useful in detecting high- frequency ultrasound vibrations, produced by the pulsed laser sources [46]. In 1963, it was observed that shock waves were formed in response to the interaction of the laser beam and water [47]. This finding catalyzed the investigations into the sound excitation in liquids and solids through pulsed laser signals. Early investigations focused on the surface effects, as the acoustic waves were produced by the laser light absorption on the surface layer of the solid or liquid.

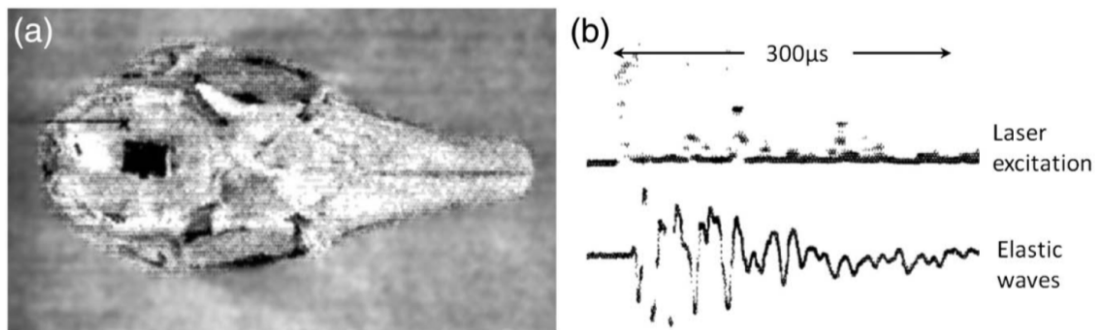


Figure 6: (a) Rabbit used in the experiment conducted by Amar et al. (b) Opto- acoustic traces from the rabbit's retina using a pulsed laser detector [48].

The first instances of photoacoustics in biomedical applications are recorded in 1964. Here, Amar et al. aimed to detect elastic ultrasound waves using laser pulses in the eye of a rabbit [48]. In 1974, it was proposed by Foster and Finch that pulsed light absorption in tissue was the cause of thermoelastic expansion, which resulted in acoustic signals [49]. This finding is

perhaps the beginning of what is mostly commonly known and used today in photoacoustic imaging. The first *in vivo* photoacoustic study was performed in 1993, where a probe was used to develop photoacoustic scans from a human finger. The laser signal emitted from the probe created alternate signals in reflection of the tissue and bone depth [50].

In 2002, Dr. John Viator illustrated the first basic ideas of photoacoustic flow cytometry through depth determination and reflective methods of epidermal melanin content [51-52]. This led to a future of imaging and cancer detection methods, which are still in working theory today [53]. In 2012, Zharov et al. developed a technique focused on ultrasensitive detection of normal blood cells in comparison to abnormal cells like circulating tumor cells. This advancement made way for the development of early cancer diagnosis, infection, and cardiovascular disorder, proving to pave the pathway of current and future detection of deadly diseases. This idea has recently been further explored through demonstrating the high sensitivity of the Cytophone technology using an *in vivo* photoacoustic flow cytometry platform for label- free detection of melanin bearing circulating tumor cells in patients with melanoma [54]. Another example of current use is the developing method to determine the bacterial content within blood samples using dyed bacteriophage being processed through photoacoustic flow cytometry [55].

1.4 PURPOSE

Although there is increasing research in the field of diagnosing various cancers through photoacoustics, incorporation and understanding of melanoma is underdeveloped. This can be attributed to a lack of knowledge around metastatic melanoma's intractability. **The main goal of this study is to understand if photoacoustic flow cytometry is a viable option for accurately detecting a heterogenous sample of melanoma cell lines.**

After melanoma has progressed beyond the skin, it first travels to the sentinel lymph node. These nodes play a role in transporting cancer cells, thus it is important to accurately detect cancer cells in these lymph nodes, before it continues to spread through other areas of the body. To do this, a lymph node biopsy is necessary. During this procedure, 6 μ m slices of the node are taken for pathology to detect the presence of cancer cells through a microscope. Because the whole node is not biopsied, there is a chance that the biopsied slice, and possibly the rest of the node, hold different characteristics. More specifically, the cancer cells may not be present in the biopsied slice, though present in other areas of the node. If this were the case, the cancer would continue to spread, and fail to be diagnosed until visible on a scan, such as a PET, MRI, or CT. When melanoma has metastasized to the point of being visible on a scan, billions of cancer cells have invaded the body, and the odds of successful treatment are slim. Thus, there needs to be a proficient way to detect and monitor melanoma after a lymph node biopsy but before scan visualization. Thus, by using a 2 cell per mL of blood threshold, it is deduced that photoacoustic flow cytometry could be an attractive method to monitor metastatic melanoma using only a blood sample. This way, a patient's exact melanoma cell count can be deduced, thus determining if further treatment is needed, prior to reaching a cancer cell concentration which would make the odds of successful treatment incredibly low.

In order to obtain the final goal, it was important to achieve smaller goals along the way. Melanoma research is primarily conducted using HS936 cells, one cell line of many that patients will present with. More commonly, a singular patient may present with multiple cell lines, depending on exact type, and mutation leading to the diagnosis. Because of this, it is important to understand the characteristics which separate the different cell lines, more specifically their

absorption. After understanding the absorption, changes in melanin content may or may not need to be performed, and understanding how to do so, is another goal of the study.

To accurately measure the final heterogenous mixture reading, it is imperative to have initial photoacoustic readings of the individual cell lines. Thus, using photoacoustic flow cytometry, combined with the approximate concentration of each sample, will provide a basis for understanding the accuracy of photoacoustic flow cytometry with each individual cell line. After initial readings are found, ensuring the survivability of the combined cell lines will be of utmost importance.

From there, the heterogenous mixture will be run through the flow cytometer, where a final reading of approximate melanoma cells will be deduced. Using the initial individual cell line readings, combined with the heterogenous mixture reading, the accuracy of photoacoustic flow cytometry in relation to real- life patient metastatic melanoma scenarios, will be concluded.

CHAPTER 2: METHODS

It is imperative to follow specific protocols for the growth and care of melanoma cells. The following methods are vital to healthy cell growth. It is also extremely important to note that these cell cultures are highly susceptible to contamination, and decontamination techniques are vital to a successful experiment.

2.1 MEDIA

Unfreeze Fetal Bovine Serum (FBS) and Penicillin Streptomycin (Pen- Strep) in a hot water bath. Unchill Dulbecco Modified Eagle Medium (DMEM) to room temperature. In a decontaminated fume hood, combine 50mL of FBS and 5mL of 100X Pen- Strep to a 500mL bottle of DMEM. Mix the contents by inverting the bottle multiple times. Then, use a vacuum filter to sterilize the prepared media. Be sure to label, and date the bottle, prior to storing it at 4°C.

2.2 CELL CULTURE

After thawing the frozen cell vials in a warm (~37°C) water bath (~2 minutes), 1000µL of the sample is pipetted into a 15mL falcon tube. 2mL of media is placed into the tube, over the course of 2 minutes. It is important to add the media slowly to not shock the cells. The media consists of 500mL of Dulbecco Modified Eagle Medium (DMEM), 50ml of Fetal Bovine Serum (FBS), and 5mL of 100x Penicillin Streptomycin (Pen- Strep). The ingredients are mixed and vacuumed into a sterilized 500mL bottle. It is stored at 4°C. After the initial 2mL is slowly added, the rest of the falcon tube is filled with media. The sample is centrifuged for ten minutes at 1600RPM. The excess media is aspirated. It is important to not disturb the pellet that has formed in the bottom of the falcon tube. 1mL of new media is added to the falcon tube. The pellet and media are gently mixed using the pipette tip. The cells and remaining media are pipetted into a

sterilized T-25 cell culture flask. Add 3mL of media to the flask. Sterilize the flask with ethanol, being mindful of the pores in the cap. The cells are then stored in an incubator at 36.5°C.

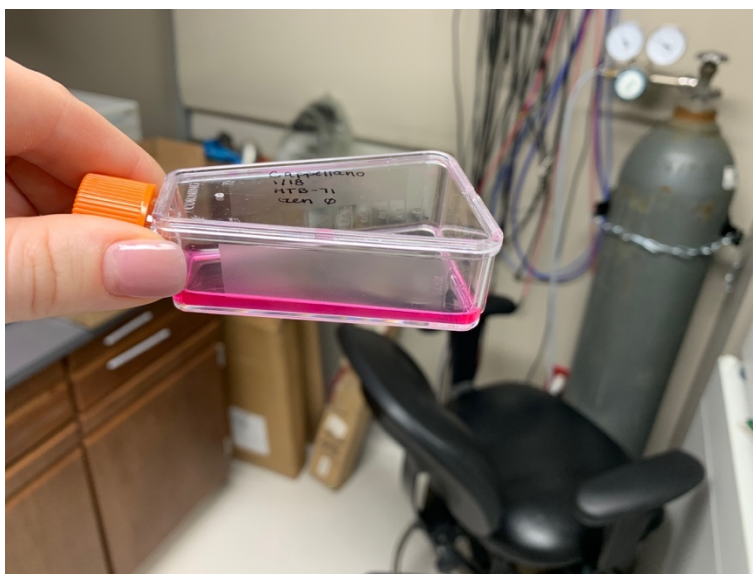


Figure 7: Freshly cultured HTB-71 cells, generation zero.

2.3 ABSORPTION

It is imperative to understand the absorption of each melanoma strand. By understanding the absorption, information about melanin content, and laser wavelength can be deduced, thus allowing one to compare each strands' characteristics. The excess media is aspirated from the T-25 cell culture flask. 3mL of 1XTrypLE™ at room temperature is then added to the flask. After about five minutes, use the microscope to see if the cells have unattached from the bottom of the flask. Light tapping of the flask may be necessary. Once the cells are unstuck, pipette 100μL out into five wells of the spectrometer well- plate, typically B1-B5 are used. In A1-A5, pipette 100μL of only 1XTrypLE™. The A1-A5 wells are used as baseline comparisons, and calibrators. Their readings should be zero. After programming the spectrometer to take a one-time absorbance read at 600nm of A1-A5 and B1-B5, place the well-plate into the machine and

run the sample. Record the absorbances.

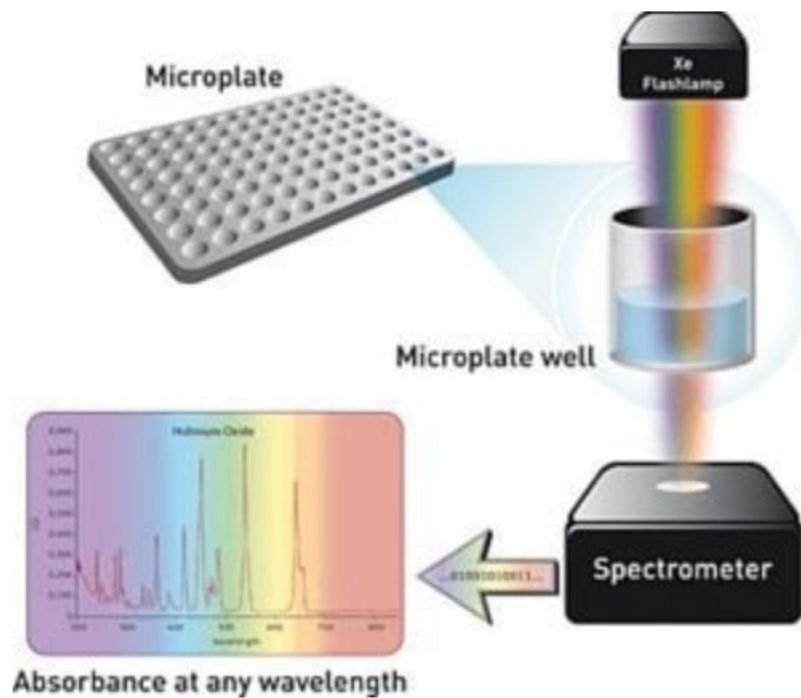


Figure 8: Microplate reader diagram. The microplate is loaded into the machine, where a Flashlamp illuminates light onto the well- plate, and the spectrometer detector deduces how much of the original light is transmitted. The absorbance is computed and converted to a visual representation on the computer [70].

The plate reader uses a light source to illuminate the sample at a specific wavelength. In this case, a 600nm wavelength was used to detect the absorbance with a one time read. An additional light source on the opposite side of the original source reads how much of the initial source reaches the detector. This value often depends on sample concentration, so it is important that all samples tested have similar cell concentrations.

1. = not stuck
1. = stuck

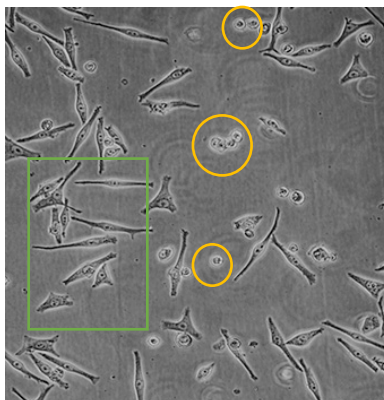


Figure 9: Microscopic image of not stuck, and stuck HS936 cells.

The remaining sample is transferred to a 15mL falcon tube filled with cell media and centrifuged for ten minutes at 1600RPM. The excess media is aspirated. It is important to not disturb the pellet that has formed in the bottom of the falcon tube. 1mL of new media is added to the falcon tube. The pellet and media are gently mixed using the pipette tip. The cells and remaining media are pipetted into a sterilized T-25 cell culture flask. Add 3mL of media to the flask. Sterilize the flask with ethanol, being mindful of the pores in the cap. The cells are then stored in an incubator at 36.5°C.

2.4 INCREASING MELANIN CONCENTRATION

After testing the absorption, it was clear that HS936 had the greatest absorbance in comparison to the other selected cell lines. Because of this, it was important to increase the absorption of the other cell lines, in order for the photoacoustic system to accurately detect the cell counts. To increase the absorption, the melanin content of the samples had to be increased.

Various studies, in addition to the understanding of cellular functions have deduced that UV radiation catalyzes pigment darkening by the chemical modification of melanin, and the distribution of melanosomes in melanocytes [63]. Because of these findings, the cell lines (except for HS936) were subject to segments of UV light. More specifically, a UVP light was

used. The light was 4 watts, with a 365nm wavelength, 0.16 Amps and 115V at 60 Hz. Each flask was placed under the lamp, for a thirty-minute interval. The lamp was kept in a backroom, with all other light sources turned off. The absorption was then tested 24 hours after initial light exposure. It took three exposure sessions to record the found results.

It is important to note that the cell lines were tested through the flow system, before and after UV treatment. Aside from the spectrometer readings, the low cytometer detections also supported the need for higher melanin concentrations.

2.5 HETEROGENOUS CULTURE

The following procedure must be done to one culture of each melanoma strand. The excess media is aspirated from the T-25 cell culture flask. 3mL of 1XTrypLE™ at room temperature is then added to the flask. After about five minutes, use the microscope to see if the cells have unattached from the bottom of the flask. Light tapping of the flask may be necessary. The remaining sample is transferred to a 15mL falcon tube filled with cell media and centrifuged for ten minutes at 1600RPM. The excess media is aspirated. It is important to not disturb the pellet that has formed in the bottom of the falcon tube. 1mL of new media is added to the falcon tube. The pellet and media are gently mixed using the pipette tip. 1mL of each falcon tube is pipetted into the same cell culture flask. After 1mL of each strand is added to the same flask, 2 mL of fresh media is added to the flask. The remaining cells are pipetted into their own unique sterilized T-25 cell culture flask. Add 3 mL of media to the flask. Sterilize the flasks with ethanol, being mindful of the pores in the cap. The cells are then stored in an incubator at 36.5°C.

2.6 PHOTOACOUSTIC FLOW CYTOMETRY

It is imperative to first calibrate the whole photoacoustic flow cytometer system. This is done by running one negative sample (oil and PBS only), then a positive sample (oil and

microspheres), followed by a negative sample until there are zero detections. After the microspheres are cleared from the system, the first step to running the sample through the flow cytometer is removing the excess media from the T-25 cell culture flask. 3mL of 1XTrypLE™ at room temperature is then added to the flask. After about five minutes, use the microscope to see if the cells have unattached from the bottom of the flask. Light tapping of the flask may be necessary. Transfer the remaining sample to a 15mL falcon tube and fill to the top with cell media. Centrifuge the sample for ten minutes at 1600RPM. Aspirate the excess media, and remember it is important to not disturb the pellet that has formed in the bottom of the falcon tube. Add 20μL of DNase to the falcon tube, followed by 2mL of histopaque. The histopaque is used to facilitate rapid recovery of viable cells from small volumes. Vortex the sample. Keep the disturbed pellet sample in the dark for fifteen minutes. After fifteen minutes, collect the entire sample into a syringe, and fill another syringe with an equal amount of oil. Place both syringes in the two-phase flow system, connected to the t- junction of the flow chamber.

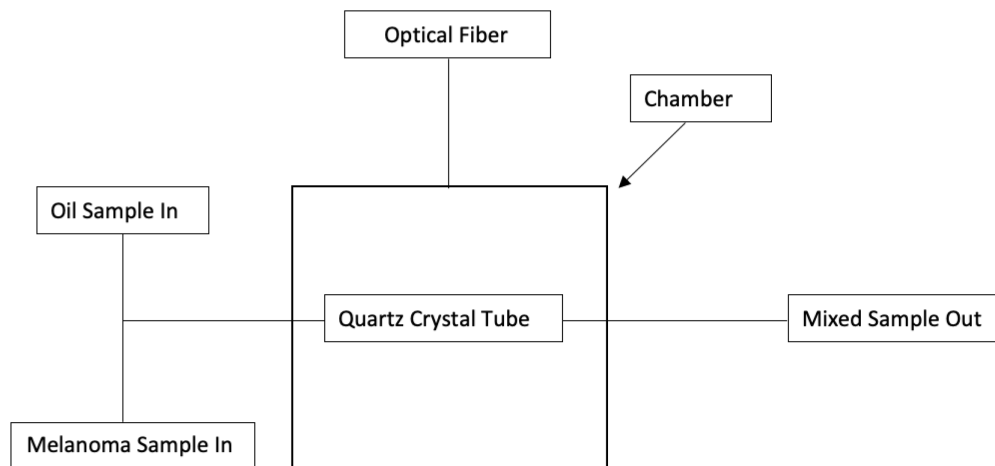


Figure 10: Schematic of a photoacoustic flow system

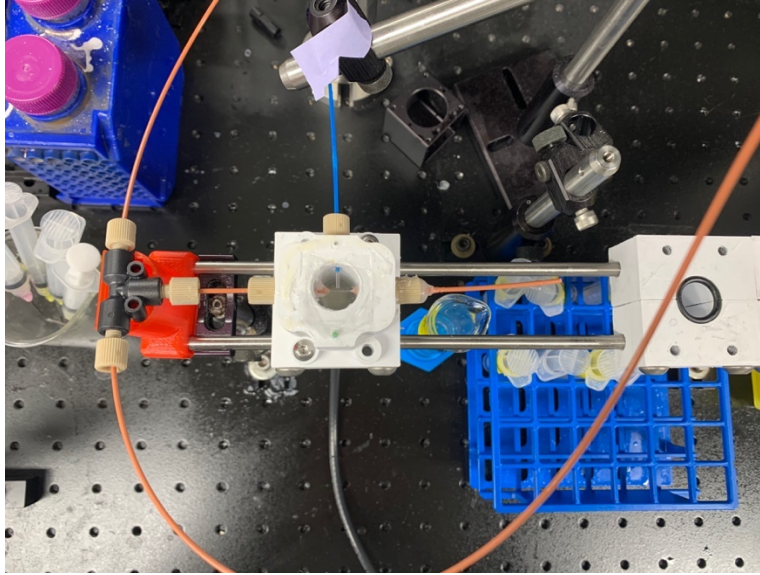


Figure 11: Top- view of the photoacoustic flow chamber, where the two orange wires on the left are the alternating flow tubes creating two phase flow generation through the quartz tube. The blue fiber optic wire introduces the flow chamber to the flashing light, catalyzing acoustic waves from cell interaction.

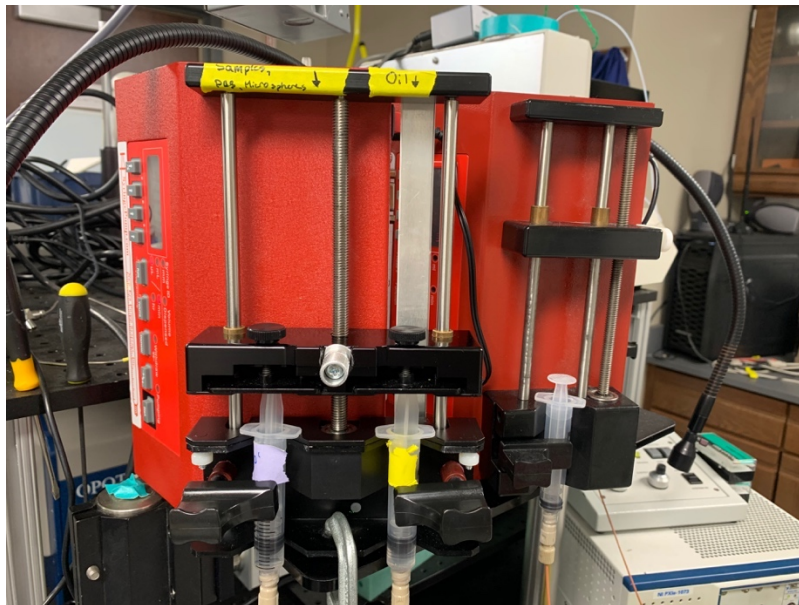


Figure 12: Two phase flow generation system

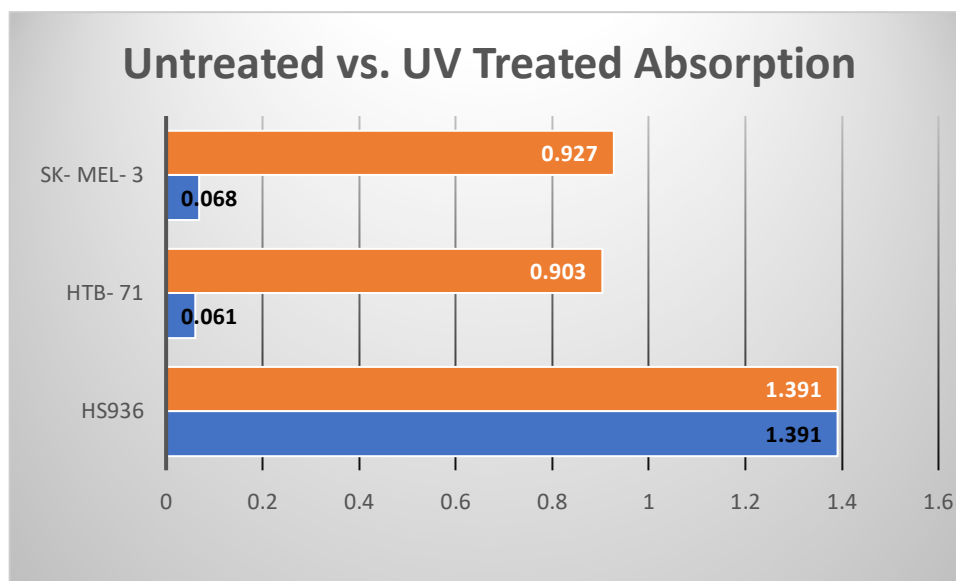
CHAPTER 3: RESULTS

3.1: OPTIMIZATION OF ABSORPTION FOR FLOW CYTOMETRY DETECTION

Melanoma Cell Line	Initial Absorption	Treated Absorption
HS936	1.391	1.391
HTB- 71	0.061	0.903
SK- MEL- 3	0.068	0.927

Table 2: Melanin concentration of various melanoma cell lines, before and after catalyzing melanogenesis.

Table 2 illustrates how upon initial absorption testing, it was clear that HS936 had the highest absorption rating, amongst all the studied lines. HS936 had an absorption of 1.391, followed by SK- MEL- 3 at 0.068, and HTB- 71 at 0.061. Thus, HTB- 71 and SK- MEL- 3 had to be UV treated in order to increase its melanin concentration, which resulted in an absorption of 0.903 and 0.927, respectively.

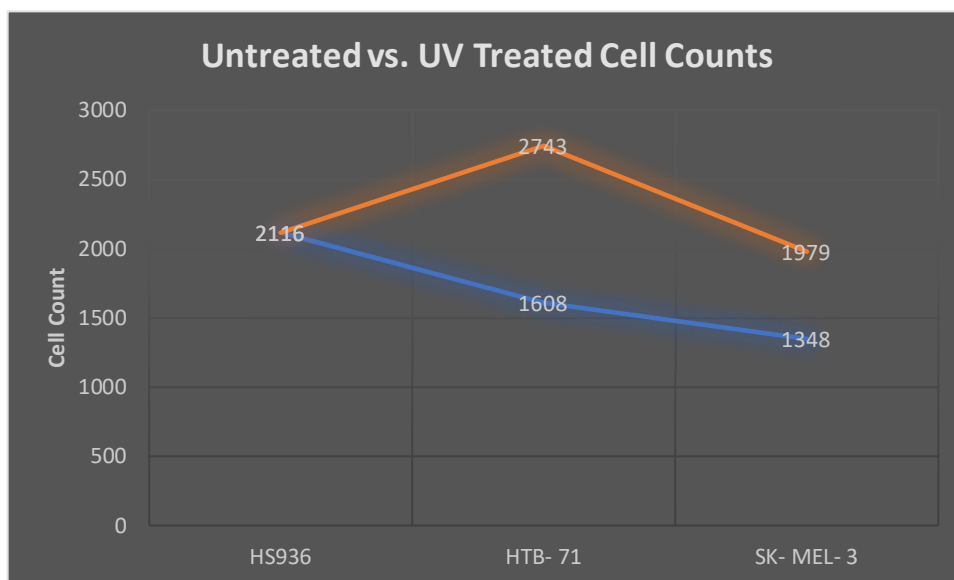


Graph 1: Melanin concentration of various melanoma cell lines, before and after catalyzing melanogenesis. Orange represents treated and blue represents untreated.

Melanoma Cell Line	Initial Detection	Treated Detection
HS936	2116	2116
HTB- 71	1608	2743
SK-MEL-3	1348	1979

Table 3: Number of melanoma cells detected, using photoacoustic flow cytometry, in relation to total concentration of untreated, and treated cell lines.

The laser initially detected 1,608 HTB- 71 cells, and 1,348 SK-MEL-3 cells. After being exposed to the UV light for a duration of time, 2,743 HTB-71 cells were detected, and 1,979 SK-MEL-3 cells. That is an average of 63.4% more melanoma cell detections when the absorbance is increased.



Graph 2: Number of melanoma cells detected, using photoacoustic flow cytometry, in relation to total concentration of untreated, and treated cell lines. Orange represents treated and blue represents untreated.

It is important to note that using a microscope, it was predicted that about 2,500 melanoma cells would be present in the tested 1 mL sample.

3.2: DETERMINING HETEROGENOUS MELANOMA CELL DETECTION

1mL of each of the three melanoma cell lines was used in the heterogenous culture. Based on the flow cytometry results from running the samples individually, it can be deduced that the sum of each individual test is the approximate number of total detections in the heterogenous mix.

$$2,116 + 2,743 + 1,979 = 6,838$$

Thus, there should be 6,838 detections, or melanoma cells, in the overall heterogenous mixture. During the test run, the flow cytometer detected 5,776 melanoma cells. **Thus, photoacoustic flow cytometry is 84.469% accurate in detecting multiple lines of melanoma in a single sample.**

$$5,776 \div 6,838 = 0.84469$$

$$= 84.469\%$$

CHAPTER 4: DISCUSSION

The overall question which this thesis is aiming to answer is ‘**can photoacoustic flow cytometry be used to accurately detect a heterogenous sample of melanoma cells?**’. The findings show that with 84.469% accuracy, photoacoustic flow cytometry can be used to detect multiple lines of melanoma within a single sample. There are various methods which may lead to a greater accuracy percentage and should be further researched.

First, one way to result in a greater melanin content than solely relying on the UV lamp, would be to expose the cells to L- Tyrosine or Tyrosinase. Studies have shown that L- Tyrosine is a substrate and positive intermediate of melanogenesis. It is a non- essential amino acid, which plays an important role in melanin pigment. In one particular study done on cultured hamster melanoma cells, an addition of 10 to 600µM of L- Tyrosine illustrated melanin synthesis and

higher tyrosinase activity [62]. In conjunction, a study performed on B16F10 mammalian melanocytes illustrated that general cellular tyrosinase activity increase when purified tyrosinase was added in doses [63]. Therefore, it can be deduced that in order for the 532nm wavelength laser to more accurately detect all melanoma cell lines, the absorption must be increased by adding either L- Tyrosine or Tyrosinase.

Second, the approximate concentrations for each sample were deduced from counting the number of cells in a 1/16 in square, through the microscope, and multiplied to approximate the total flask concentration. It would be most accurate to use an automated cell counter, and thus be able to compare the detected cell count, to the exact concentration count. Although visual concentrations are assumed to be relatively accurate, it would be most helpful to have exact counts through the automated machine.

It should also be noted that there could have been a loss of cells in the recovery process. For example, when the initial HS936 sample was run, the sample was re- collected from the output of the flow chamber and reused for the heterogenous mix. When the HS936 sample was run through the laser initially, the output is mixed with oil from the two- phase flow chamber. Using a syringe, the cell sample was suctioned out of the tube which it was caught in. This was possible due to the different densities of the sample and oil, making a separation clear. Though through this collection process, there may have been cells left in the oil density, and not recollected for the heterogenous mix. This may attribute to the lower cell count in the heterogenous mix.

4.1: FUTURE ADVANCEMENTS

There is a clear clinical need for a more accurate method to detect and monitor metastatic melanoma between a lymph node biopsy, and visual scan confirmation. As previously discussed,

current methods are often inaccurate, missing a progressive diagnosis, and failing to treat the disease in a timely manner. This method is able to accurately detect circulating tumor cells, that are too small to show up on a scan, though may have been missed in a lymph node biopsy. Between preparing the sample, and running it through the flow chamber, the total time taken is less than thirty minutes. Results are accurate to the point of exact tumor cell count, and thus can diagnosis exact stage, or be used for understanding the progression of treatment. By making this method accessible in a clinical setting, it is clear that patients would be preserving, often life-saving, time.

There are three primary developments that need to be made in order to implement photoacoustic flow cytometry in a clinical setting. The first development is a greater understanding for the wavelengths and absorbances of different melanoma cell lines. The most commonly known and understood cell line is HS936. There are over 100 types of melanoma cell lines, and though there is an understanding and recognition of them, there is a lack of evidence towards their characteristics that would be needed to conduct flow cytometry [59]. More specifically, the absorbance and wavelengths of said cell lines must be known in order for the laser to be calibrated correctly, to best detect all possible cells. Although this thesis does address this concern, more research is still needed. More specifically, three unique cell lines were investigated, though there are many more that still hold unknown characteristics. A continued understanding of these cell lines are critical for photoacoustic flow cytometry to be used in a clinical setting as a valid detection and monitoring method.

Secondly, there needs to be new or alternative acoustic gel. The gel lubricates the KTP crystal flow chamber and aids in dispersing the light energy. When applying the gel to the flow chamber, there are often many bubbles present. It is incredibly important to remove these

bubbles, in order to receive the most accurate cell count reading. Often times, if there are bubbles present, the detections are increased, and the wavelength threshold is affected. In addition, it would be useful to develop more permanent flow chambers to ensure acoustic coupling.

Lastly, a clearer understanding of the necessary concentration for detection would be useful for further developments. The concentration of each cell line in the specific experiments performed was approximately 10^4 cells per flask. By performing dilution intervals and understanding the accuracy of detection, critical information will be gained about the laser specificity. These findings will relate to more real-life examples of what melanoma concentrations may be within patients' blood samples. In addition, the findings can be used to further advance the accuracy of the laser, and its ability to detect alternate types of cancers or cellular conditions.

4.2: CONCLUSION

In conclusion, photoacoustic flow cytometry can detect multiple melanoma cell lines in a singular sample with 84.469% accuracy. These findings are imperative to developing a better method to detect and monitor metastasized melanoma, before it is too late for treatment.

By knowing the individual cell lines absorbance, it was possible to use UV light to increase certain absorbances in order for the cells to best be detected by the chosen 532nm wavelength. From there, it was imperative to run each cell line individually to get an initial cell count, prior to running the samples together, in a heterogenous sample.

Although there was a slight loss of cells between the individual and heterogenous sample run, improved methods could aid in decreasing this loss, and thus increasing the overall accuracy, possibly above 90% detection. These improved methods include cell and oil recovery, new acoustic gel, and the implementation of L- tyrosine or tyrosinase. Further investigations

should also include understanding the absorbance threshold for melanoma and the 532nm wavelength laser.

Ultimately, it can be deduced that photoacoustic flow cytometry could be a viable, and attractive method to improve the detection and monitoring process of metastatic melanoma in clinical patients.

APPENDIX

Melanoma Cell Culturing Protocols

Our cells:

1. HS936
2. HTB- 71
3. SK- MEL- 3

Incubator:

1. Set the temperature of the incubator to 36.5°C
 1. Temperatures greater than 37°C leads to cell death
2. Set the incubator to maintain 5.0% CO₂

Media:

1. Unfreeze FBS (Fetal Bovine Serum) and Pen-Strep (Penicillin Streptomycin)
 1. Both FBS and Pen-Strep are kept frozen in -20°C
2. Unchill DMEM (Dulbecco Modified Eagle Medium) to approximately room temperature
 1. DMEM is found in the fridge (4°C)
3. Add
 1. 50 mL FBS
 2. 5 mL 100X Pen-Strepto a 500 mL bottle of DMEM
3. Mix the contents by inverting the bottle a few times
4. Vacuum filter the media into a sterilized 500 mL bottle
5. Label / Date bottle

6. Store in fridge (4°C)

Unfreezing cells:

1. Unchill the media to room temperature
2. Close hood and turn on UV light
3. Open hood and turn on the blower of the hood
4. Wipe down everything inside of the hood and everything being used (including the outside of the media bottle and the pipette) with 70% ethanol
5. Place the frozen cell vial in warm (~37°C) water until thawed (≈2 min)
6. Add 1000 µL of sample into a 15 mL falcon tube
7. Add 2 mL of media 1 drop at a time over the course of about 2 minutes to not shock the cells
8. Gently add the rest of the media until the tube is filled
9. Centrifuge for 10 minutes at 414 RCF (1600 RPM in lab centrifuge), being sure to balance the centrifuge
10. Aspirate excess media, being careful not to disturb the pellet
11. Add 1 mL of new media to falcon tube
12. Mix the pellet and media gently with the pipette
13. Pipette cells and media into a sterilized T-25 cell culture flask
14. Add 3 mL of media
15. Label flask and incubate at 36.5°C / 5.0% CO₂
 1. Strain, date, initials, Gen 0
16. Turn off blower
17. Close hood and turn on UV light

Changing Media

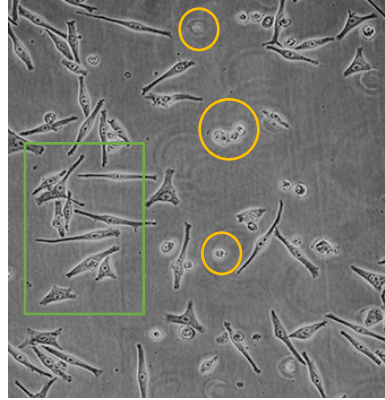
1. Media is typically changed every 2-3 days
2. Media turns yellow/orange when it becomes more acidic → needs to be changed
3. When a flask becomes extremely concentrated with cells (a confluent layer of cells stuck to the flask), replace media with 5 mL
4. Be cautious in avoiding contamination of the flasks or media

1. Unchill the media to room temperature
2. Close hood and turn on the UV light
3. Open the hood and turn on the blower
4. Wipe down everything inside of the hood and everything being used with 70% ethanol
5. Pipette out old media
 1. Can wash down sink if rinsed with water afterwards
6. Pipette in 4 mL of media (with a clean pipette)
7. Return cells to incubator
8. Turn off blower
9. Close hood and turn on UV light

Splitting the Cells

1. Track cell growth daily or every other day to determine when to split the cells
2. Split the cells if their growth has leveled off and 60-80% of the cells are stuck to the bottom of the flask

○ = not
stuck
□ = stuck



3. Split the cells if there is a confluent layer stuck to the bottom
1. Unchill the media and 1X TrypLE™ to room temperature
2. Close hood and turn on the UV light
3. Open the hood and turn on the blower
4. Wipe down everything inside of the hood and everything being used with 70% ethanol
5. Pipette out the media
6. Add 3 mL of TrypLE
 1. Wait 5 minutes
 2. Look under the microscope to see if the cells have unattached from the bottom of the flask
 3. The flask might need tapped / flicked to completely lift the cells
7. Pipette out the TrypLE and cells into a 15 mL falcon tube
8. Fill the falcon tube to the top with media
9. Centrifuge for 10 minutes at 1600 RPM, being sure to balance the centrifuge
10. Remove excess media, being careful not to disturb the pellet
11. Resuspend pellet with 3 mL of media for each flask the cells are being split into
 1. If you are splitting the cells into 2 flasks, resuspend with 6 mL of media

12. Gently mix cells and media with the pipette
13. Pipette the cells and 3 mL of media into each sterile flask
14. Add 1 mL of media to each flask for a total of 4 mL of media in each flask
15. Label with Strain/Date/Initial/Gen "x"
16. Turn off blower
17. Close hood and turn on UV light

Freezing the Cells

18. Our cells have about a 20-40% recovery rate
-
1. Unchill the media and 1X TrypLE to room temperature
 2. Place FBS and DMSO in a hot water bath until they are unfrozen
 1. FBS is kept in the freezer
 2. DMSO is kept in the fridge
 3. Close hood and turn on the UV light
 4. Open the hood and turn on the blower
 5. Wipe down everything inside of the hood and everything being used with 70% ethanol
 6. Pipette out the media
 7. Add 3 mL of TrypLE
 1. Wait 5 minutes
 2. Look under the microscope to see if the cells have unattached from the bottom of the flask
 3. The flask might need tapped / flicked to completely lift the cells
 8. Pipette out the TrypLE and cells into a 15 mL falcon tube

9. Fill the falcon tube to the top with media
10. Centrifuge for 10 minutes at 414 RCF (1600 RPM in lab centrifuge), being sure to balance the centrifuge
11. Remove excess media, being careful not to disturb the pellet
12. Label 2 mL freezer tubes (3 per flask) with cell name
13. Add 3 mL of FBS to the cell clump and then mix
14. Add 100 μ L of DMSO to each 2 mL freezer tube
15. Add 1 mL of FBS and cells to each of the 2 mL freezer tubes
16. Briefly vortex each tube on the lowest setting
17. Place tubes in a freezer container and place in the -80.0°C freezer
18. Discard cell flasks
19. Turn off blower
20. Close hood and turn on UV light

REFERENCES

1. Cancer facts & Figures 2010. (n.d.). Retrieved March 02, 2021, from <https://www.cancer.org/research/cancer-facts-statistics/all-cancer-facts-figures/cancer-facts-figures-2010.html>
2. Clark, W. H., Jr, Elder, D. E., Guerry, D., 4th, Epstein, M. N., Greene, M. H., & Van Horn, M. (1984). A study of tumor progression: the precursor lesions of superficial spreading and nodular melanoma. *Human pathology*, 15(12), 1147–1165.
[https://doi.org/10.1016/s0046-8177\(84\)80310-x](https://doi.org/10.1016/s0046-8177(84)80310-x)
3. Brunet, A., Roux, D., Lenormand, P., Dowd, S., Keyse, S., & Pouyssegur, J. (1999). Nuclear translocation of p42/p44 mitogen-activated protein kinase is required for growth factor-induced gene expression and cell cycle entry. *The EMBO journal*, 18(3), 664–674.
<https://doi.org/10.1093/emboj/18.3.664>
4. Davies, H., Bignell, G. R., Cox, C., Stephens, P., Edkins, S., Clegg, S., Teague, J., Woffendin, H., Garnett, M. J., Bottomley, W., Davis, N., Dicks, E., Ewing, R., Floyd, Y., Gray, K., Hall, S., Hawes, R., Hughes, J., Kosmidou, V., Menzies, A., ... Futreal, P. A. (2002). Mutations of the BRAF gene in human cancer. *Nature*, 417(6892), 949–954.
<https://doi.org/10.1038/nature00766>
5. Patton, E. E., Widlund, H. R., Kutok, J. L., Kopani, K. R., Amatruda, J. F., Murphey, R. D., Berghmans, S., Mayhall, E. A., Traver, D., Fletcher, C. D., Aster, J. C., Granter, S. R., Look, A. T., Lee, C., Fisher, D. E., & Zon, L. I. (2005). BRAF mutations are sufficient to promote nevi formation and cooperate with p53 in the genesis of melanoma. *Current biology : CB*, 15(3), 249–254.
<https://doi.org/10.1016/j.cub.2005.01.031>

6. Thompson, J. F., Scolyer, R. A., & Kefford, R. F. (2005). Cutaneous melanoma. *Lancet (London, England)*, 365(9460), 687–701. [https://doi.org/10.1016/S0140-6736\(05\)17951-3](https://doi.org/10.1016/S0140-6736(05)17951-3)
7. Hussussian, C. J., Struewing, J. P., Goldstein, A. M., Higgins, P. A., Ally, D. S., Sheahan, M. D., Clark, W. H., Jr, Tucker, M. A., & Dracopoli, N. C. (1994). Germline p16 mutations in familial melanoma. *Nature genetics*, 8(1), 15–21. <https://doi.org/10.1038/ng0994-15>
8. Hodgkinson, C. A., Moore, K. J., Nakayama, A., Steingrímsson, E., Copeland, N. G., Jenkins, N. A., & Arnheiter, H. (1993). Mutations at the mouse microphthalmia locus are associated with defects in a gene encoding a novel basic-helix-loop-helix-zipper protein. *Cell*, 74(2), 395–404. [https://doi.org/10.1016/0092-8674\(93\)90429-t](https://doi.org/10.1016/0092-8674(93)90429-t)
9. King, R., Weilbaecher, K. N., McGill, G., Cooley, E., Mihm, M., & Fisher, D. E. (1999). Microphthalmia transcription factor. A sensitive and specific melanocyte marker for MelanomaDiagnosis. *The American journal of pathology*, 155(3), 731–738. [https://doi.org/10.1016/S0002-9440\(10\)65172-3](https://doi.org/10.1016/S0002-9440(10)65172-3)
10. Garraway, L. A., Widlund, H. R., Rubin, M. A., Getz, G., Berger, A. J., Ramaswamy, S., Beroukhi, R., Milner, D. A., Granter, S. R., Du, J., Lee, C., Wagner, S. N., Li, C., Golub, T. R., Rimm, D. L., Meyerson, M. L., Fisher, D. E., & Sellers, W. R. (2005). Integrative genomic analyses identify MITF as a lineage survival oncogene amplified in malignant melanoma. *Nature*, 436(7047), 117–122. <https://doi.org/10.1038/nature03664>
11. Haass, N. K., Smalley, K. S., Li, L., & Herlyn, M. (2005). Adhesion, migration and communication in melanocytes and melanoma. *Pigment cell research*, 18(3), 150–159. <https://doi.org/10.1111/j.1600-0749.2005.00235>

12. Bienz M. (2005). beta-Catenin: a pivot between cell adhesion and Wnt signalling. *Current biology : CB*, 15(2), R64–R67.
<https://doi.org/10.1016/j.cub.2004.12.058>
13. Satyamoorthy, K., Muyrers, J., Meier, F., Patel, D., & Herlyn, M. (2001). Mel-CAM-specific genetic suppressor elements inhibit Melanoma growth and invasion through loss of gap junctional communication. *Oncogene*, 20(34), 4676-4684.
[doi:10.1038/sj.onc.1204616](https://doi.org/10.1038/sj.onc.1204616)
14. Miller, A. J., & Mihm, M. C., Jr (2006). Melanoma. *The New England journal of medicine*, 355(1), 51–65. <https://doi.org/10.1056/NEJMra052166>
15. “[International School of Photonics: Research: Photoacoustics: Photoacoustic Effect |.” | International School of Photonics | Research | Photoacoustics | Photoacoustic Effect |, photonics.cusat.edu/Research_Photoacoustics.html.
16. Ntziachristos V (2010) Going deeper than microscopy: the optical imaging frontier in biology. *Nature Methods* 7: 603-614. doi: 10.1038/nmeth.1483
17. Ntziachristos V et al. (2005) Looking and listening to light: the evolution of whole-body photonic imaging. *Nature Biotechnology* 23: 313-320. doi: 10.1038/nbt1074
18. Oscilloscope. (n.d.). Retrieved March 02, 2021, from <http://www.merriam-webster.com/dictionary/oscilloscope>
19. Sigrist, M. W., (1999). Photoacoustic spectroscopy, method and instrumentation, *Encyclopaedia of spectroscopy and spectrometry*. 3:1810.
20. Patel, C. K., & Tam, A. C. (1981). Pulsed optoacoustic spectroscopy of condensed matter. *Reviews of Modern Physics*, 53(3), 517-550. doi:10.1103/revmodphys.53.517

21. Kinney J. B., Staley R. H. (1982) Applications of Photoacoustic Spectroscopy. *Annual Review of Material Science*. 12:295.
22. Tam, A. C., Photoacoustics: Spectroscopy and other applications. *Ultrasensitive laser spectroscopy*, chapter 1, New York: Academic Press.12-50
23. Pao, Y. (2012). *Optoacoustic Spectroscopy and Detection*. Burlington: Elsevier Science.
24. Mandelis, A. (Ed.). (1992). *Principles and perspectives of photothermal and photoacoustic phenomena (Progress in photothermal and photoacoustic science and technology)* (Vol. 1, pp. 455-510). Elsevier.
25. Tam, A. C., Application of photoacoustic sensing techniques. *Review of modern physics* 58:381.
26. Nelson, E. T., & Patel, C. K. (1981). Response of piezoelectric transducers used in pulsed optoacoustic spectroscopy. *Optics Letters*, 6(7), 354. doi:10.1364/ol.6.000354
27. Haisch, C. and Niessne, R. (2002) Light and Sound - Photoacoustic spectroscopy. *Spectroscopy Eur*. 14(5):10
28. Gregoriou V. Photoacoustic Spectroscopy. Available: <http://nteserveur.univ-lyon1.fr/spectroscopie/gbdo/spedagogiques.html>
29. Schmid, T. Photoacoustic spectroscopy for process analysis. *Anal Bioanal Chem* **384**, 1071–1086 (2006). <https://doi.org/10.1007/s00216-005-3281-6>
30. Ball, D W. (2006) The Baseline Photoacoustic Spectroscopy. *Spectroscopy*, 21:14-16.
31. MIMS, III, F. M. (1980). Alexander Graham Bell and the Photophone: The centennial of the invention Of Light-Wave Communications, 1880–1980. *Optics News*, 6(1), 8. doi:10.1364/on.6.1.000008

32. Bell, A. G. (1881). Production of sound by radiant energy. *Journal of the Franklin Institute*, 111(6), 401-428. doi:10.1016/0016-0032(81)90005-3
33. Bell, A. G. (1881). The spectrophone. In *The spectrophone* (Vol. 4). Washington: Smithsonian Inst.
34. Mercadier, E. (1881) “Sur la radiophonie,” J. Phys. Theor. Appl. **10**, 53–68.
35. Mercadier, E. (1881) “Sur la radiophonie,” J. Phys. Theor. Appl. **10**, 53–68.
36. Preece, W. H. (1881). On the conversion of radiant energy Into SONOROUS VIBRATIONS 1. *Nature*, 23(595), 496-497. doi:10.1038/023496a0
37. Veingerov, M.L. (1938) “A method of gas analysis based on the Tyndall-Röntgen optico-acoustic effect,” Dokl. Akad. Nauk SSSR **19**, 687–688.
38. Luft, K.F. (1975). Infrared technqiues for the measurement of carbon monoxide. *Ann. Occup. Hyg.* 18: 45-51.
39. M. L. Veingerov, “Spectrophone - an instrument for investigation of infrared absorption spectra of gases and for quantitative and qualitative spectrum analysis of multicomponent gas mixtures,” Dokl. Akad. Nauk SSSR **46**, 182 (1945)
40. G. Gorelik, “On a possible method of studying the energy exchange time between the different degrees of freedom of molecules in a gas,” Dokl. Akad. Nauk SSSR **54**, 779 (1946)
41. P. V. Slobodskaya, “Determination of the energy transfer rate from vibrational to translational molecular motion by means of a spectrophone,” Izvest. Akad. Nauk SSSR **12**, 656–662 (1948)
42. B. I. Stepanov and O. P. Girin, Zh. Eksp. Teor. Ftz. **20**, 947 (1950)

43. Cottrell, T. L. (1950). The absorption of interrupted infra-red radiation. *Transactions of the Faraday Society*, 46, 1025-1030. doi:10.1039/tf9504601025
44. Cottrell, T. L., Macfarlane, I. M., Read, A. W., & Young, A. H. (1966). Measurement of Vibrational relaxation times by the spectrophone. application TO CH₄, CO₂, N₂O, CO, NH₃ and HCN. *Transactions of the Faraday Society*, 62, 2655.
doi:10.1039/tf9666202655
45. Kerr, E. L., & Atwood, J. G. (1968). The laser illuminated absorptivity spectrophone: a method for measurement of weak absorptivity in gases at laser wavelengths. *Applied optics*, 7(5), 915–921. <https://doi.org/10.1364/AO.7.000915>
46. Curie, J. (1880). *Développement par pression de l'électricité polaire dans les cristaux hémihédres à faces inclinées* (Vol. 91, pp. 294-295).
47. Askaryan, G. A., Prokhorov, A. M., Chanturia, G. F., & Shipulo, G. P. (1963). Propagation of a laser beam through a liquid. *Journal of Experimental and Theoretical Physics*, (44), 2180-2182.
48. Amar, L., Bruma, M., Desyignes, P., Leblanc, M., Perdriel, G., & Velghe, M. (1964). Detection, d'ondes élastiques (ultrasonores) sur l'os occipital, induites par impulsions laser dans l'oeil d'un lapin. *Academy of Sciences*, (259), 3653-3655.
49. Foster, K. R., & Finch, E. D. (1974). Microwave hearing: Evidence for thermoacoustic auditory stimulation by pulsed microwaves. *Science*, 185(4147), 256-258.
doi:10.1126/science.185.4147.256
50. Chen, Q., Dewhurst, R., Payne, P., & Davies, A. (1993). Photo-acoustic probe for intra-arterial imaging and therapy. *Electronics Letters*, 29(18), 1632-1633.
doi:10.1049/el:19931087

51. Viator, J. A., Au, G., Paltauf, G., Jacques, S. L., Prahl, S. A., Ren, H., . . . Stuart Nelson, J. (2002). Clinical testing of a photoacoustic probe for port wine stain depth determination. *Lasers in Surgery and Medicine*, 30(2), 141-148. doi:10.1002/lsm.10015
52. Viator, J. A., Komadina, J., Svaasand, L. O., Aguilar, G., Choi, B., & Stuart Nelson, J. (2004). A Comparative Study of Photoacoustic and Reflectance Methods for Determination of Epidermal Melanin Content. *Journal of Investigative Dermatology*, 122(6), 1432-1439. doi:10.1111/j.0022-202x.2004.22610.
53. Weight, R. M., Viator, J. A., Dale, P. S., Caldwell, C. W., & Lisle, A. E. (2006). Photoacoustic detection of metastatic melanoma cells in the human circulatory system. *Optics letters*, 31(20), 2998–3000. <https://doi.org/10.1364/ol.31.002998>
54. Galanzha, E. I., Menyaev, Y. A., Yadem, A. C., Sarimollaoglu, M., Juratli, M. A., Nedosekin, D. A., . . . Zharov, V. P. (2019). In vivo liquid biopsy using Cytophone platform for photoacoustic detection of circulating tumor cells in patients with melanoma. *Science Translational Medicine*, 11(496). doi:10.1126/scitranslmed.aat5857
55. Edgar, R. H., Cook, J., Noel, C., Minard, A., Sajewski, A., Fitzpatrick, M., . . . Viator, J. A. (2019). Bacteriophage-mediated identification of bacteria using photoacoustic flow cytometry. *Journal of Biomedical Optics*, 24(11), 1. doi:10.1117/1.jbo.24.11.115003
56. Paschotta, R. (2008). Saturable Absorbers. *Encyclopedia of Laser Physics and Technology*, 1.
57. Hollas, M. J. (2004). Some Important Results in Quantum Mechanics. In *Modern Spectroscopy* (Fourth ed., pp. 1-5). Chichester, West Sussex: John Wiley & Sons.
58. How does a spectrometer work? (n.d.). Retrieved February 22, 2021, from <https://bwtek.com/spectrometer-introduction/>

59. Melanoma Cell Lines & Mutations. (n.d.). Retrieved February 22, 2021, from <https://rockland-inc.com/melanoma-cell-lines.aspx>
60. Laser principles. (n.d.). Retrieved February 22, 2021, from https://www.keyence.com/ss/products/marketing/marketing_central/study/principle.jsp
61. Slominski, A., Zmijewski, M. A., & Pawelek, J. (2012). L-tyrosine and L-dihydroxyphenylalanine as hormone-like regulators of melanocyte functions. *Pigment cell & melanoma research*, 25(1), 14–27. <https://doi.org/10.1111/j.1755-148X.2011.00898>.
62. Zaidi, K. U., Ali, S. A., & Ali, A. S. (2016). Effect of purified mushroom tyrosinase on melanin content and melanogenic protein expression. *Biotechnology Research International*, 2016, 1-8. doi:10.1155/2016/9706214
63. Maddodi, N., Jayanthi, A., & Setaluri, V. (2012). Shining light on skin pigmentation: the darker and the brighter side of effects of UV radiation. *Photochemistry and photobiology*, 88(5), 1075–1082. <https://doi.org/10.1111/j.1751-1097.2012.01138>.
64. Vincent K., Postovit L. Investigating the utility of human melanoma cell lines as tumour models. *Oncotarget*. 2017; 8: 10498-10509. Retrieved from <https://www.oncotarget.com/article/14443/text/>
65. Tirosh, I., Izar, B., Prakadan, S. M., & Wadsworth, M. H., II. (2016). Dissecting the multicellular ecosystem of metastatic melanoma by single-cell RNA-seq. *Science*, 354(6282), 189-196. doi:10.1126/science.aad0501
66. Gilchrest, B. A., Park, H. Y., Eller, M. S., & Yaar, M. (1996). Mechanisms of ultraviolet light-induced pigmentation. *Photochemistry and photobiology*, 63(1), 1–10. <https://doi.org/10.1111/j.1751-1097.1996.tb02988.x>

67. Ball, D. W. (2006). *Field guide to spectroscopy*. Bellingham, WA, WA: SPIE Press.
68. IUPAC. (2021, February 18). Beer lambert law: Transmittance & absorbance. Retrieved March 09, 2021, from <https://www.edinst.com/us/blog/the-beer-lambert-law/>
69. IUPAC. (2021, January 25). Spectrometer: What is a spectrometer?: Types of spectrometers. Retrieved March 09, 2021, from <https://www.edinst.com/us/blog/what-is-a-spectrometer/>
70. Uv/vis spectrometer in a microplate reader: Bmg labtech. (n.d.). Retrieved March 16, 2021, from <https://www.bmglabtech.com/uv-vis-spectrometer/>